MAX-PLANCK-INSTITUT FÜR PLASMAPHYSIK

GARCHING BEI MÜNCHEN

A SCRAPE-OFF LAYER BASED MODEL FOR HUGILL-GREENWALD TYPE DENSITY LIMITS

K. BORRASS, R. SCHNEIDER, R. FARENGO

IPP 5/70 August 1996

Die nachstehende Arbeit wurde im Rahmen des Vertrages zwischen dem Max-Planck-Institut für Plasmaphysik und der Europäischen Atomgemeinschaft über die Zusammenarbeit auf dem Gebiete der Plasmaphysik durchgeführt.

A SCRAPE-OFF LAYER BASED MODEL FOR HUGILL-GREENWALD TYPE DENSITY LIMITS

K. BORRASS, R. SCHNEIDER

Max-Planck-Institut für Plasmaphysik,
Garching/Munich,
Germany

R. FARENGO

Centro Atomico Bariloche,
Bariloche, Rio Negro,
Argentina

ABSTRACT. In present tokamaks the density limit is observed to coincide with complete divertor detachment. This paper presents a scrape-off layer based model for this "detachment limit". Emphasis is placed on understanding the power independent, $1/q$-type scaling (Hugill-Greenwald type scaling) observed in many divertor machines. A simple analytical model for the SOL, complemented by dimensional considerations on gas targets, is used to describe the underlying mechanism and derive scalings for the critical density. Physically, the power independent regime is associated with an intermediate transverse neutral collisionality in the divertor. Extensive B2-EIRENE studies were conducted to verify the analytical considerations. Computational results are compared with experimental findings on JET. Possible ways to access the power dependent regime are discussed.

1. INTRODUCTION

Historically, various mechanisms that limit the accessible operation window of a tokamak with respect to density have been subsumed under the concept of a density limit (DL). In most cases DLs are manifested as a disruptive limit. When approaching the disruptive DL, one normally goes through a sequence of events, starting possibly in the scrape-off layer (SOL), including formation of Marfes and ending in an $m = 2$, $n = 1$ disruption. Density limit studies may widely differ by focussing on different steps of this sequence. The most general and most ambitious approach aims at a complete understanding of the whole sequence of events leading to a disruption. An attempt of this kind was made in Ref. [1] for limiter machines. The present paper is confined to describing only the starting event in the sequence (onset condition), which is sufficient if one is mainly interested in determining the actual operation window of a device. It is emphasized that this is a purely pragmatic decision.

Initially, DLs were described as limits for the line averaged density, which can easily be determined. As edge diagnostics improved, evidence evolved from a number of machines that density limits are actually limits on the upstream edge density n_S [2, 3]. From a theoretical point of view, the steady-state edge solution space is not naturally bound with respect to n_S. This means that, for given machine parameters and boundary conditions, one can, in principle, obtain arbitrarily high n_S values by increasing, for instance, the particle content in the system. An upper bound must result from an additional constraint that limits the accessible part of the solution space (threshold condition). Possible threshold conditions might be the onset condition of a thermal instability in the divertor [4] or the occurrence of a Marfe. A special situation is given if the threshold condition can be formulated in terms of edge quantities alone. It is exactly this situation where the wording "edge based density limit" is appropriate. Normally threshold conditions are not naturally given in terms of parameters appearing in density limit scalings, such as power across the separatrix, safety factor, field etc., and the non-trivial part of deriving SOL based DL models consists in, apart from identifying the right threshold mechanism, combining the threshold condition with edge theory and translating it into a usable format.

During the past few years it has become apparent that divertor detachment is a ubiquitous phenomenon in high-density divertor discharges and that divertor discharges go through a detached state before the DL is reached. Here detachment includes a pressure drop along B (momentum detachment) [5], a drop of the target power flux (energy detachment) and a drop of the target particle flux (or ion saturation current I_{sat}, particle detachment). While momentum and energy detachment start at temperatures $T_e \leq 5$eV, where charge exchange and elastic collisions become effective, particle detachment starts at temperatures $T_e \leq 1.5$eV through the effect of recombination [6] and it defines the final state, where the plasma virtually loses contact with the plate. In what follows we define complete detachment as the condition where the particle flux (or I_{sat}) has dropped by about one order of magnitude in at least one divertor leg. There is much experimental evidence that the maximum upstream separatrix density is reached precisely when full detachment is achieved. This suggests using complete detachment as the threshold condition (detachment limit). This is clearly an edge condition in the sense described above. The correlation between DL and complete detachment, which is illustrated in Fig. 1 with a typical JET density limit discharge, has been explicitly verified for a large number of JET and ASDEX Upgrade discharges.

Simple density limit scalings have been used as a convenient way to summarize experimental findings and predictions from theoretical models. One of the earliest scalings, based on DITE ohmic and additionally heated discharges, was proposed by Hugill et al. [7]:

$$\bar{n}^{crit} = c_{Hugill}\frac{B_t}{Rq_\psi} \tag{1}$$

where $\bar{n}$ is the critical line averaged density, B_t the toroidal field on axis, R the major radius and q_ψ the edge safety factor ($c_{Hugill} \simeq 1.82$ if n is in $10^{20}\mathrm{m}^{-3}$, B_t in T and R in m). With $q_\psi = \frac{2\pi}{\mu_0}\frac{a^2 B_t}{RI_p}g$, where I_p is the plasma current, a the plasma minor

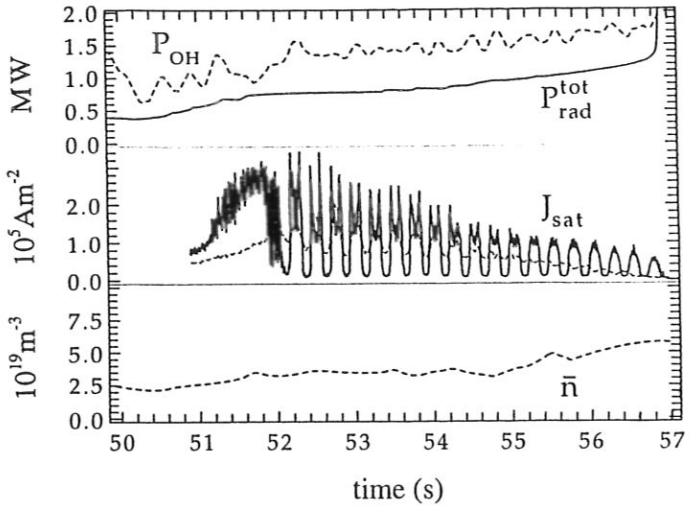

FIG. 1. *Time traces of line averaged density $\bar{n}$, heating power P_{heat}, total radiation power P_{rad}^{tot} and ion saturation current I_{sat} from an inboard, near-separatrix Langmuir probe for a typical JET density limit discharge.*

radius and g a factor that characterizes the plasma shape, one gets

$$\bar{n}^{crit} = C_{Hugill}\frac{I_p}{\pi a^2}\frac{1}{g} \tag{2}$$

where $C_{Hugill} = 1.14$ if n is in $10^{20}\mathrm{m}^{-3}$, I_p in MA and a in m. A slightly different version was derived by Greenwald from an inter-machine comparison [8]. It is obtained from Eq. (2) by making the substitution $C_{hugill} \rightarrow 1$ and $g \rightarrow 1$.

DL scalings of the Greenwald-Hugill type, the most striking features of which are the weak or vanishing power dependence and a $1/q$-dependence, are typically found in divertor tokamaks [2, 7, 9]. A rather different type of scaling is observed in limiter machines [3, 10, 11, 12, 13] and a small number of tokamaks [14]. The picture is less coherent but common elements are an approximate square root power dependence and a weak or vanishing inverse q-dependence.

Both versions of power dependence and q-dependence can be interpreted as special cases of a general class of scalings given by (we restrict ourselves for the moment to power dependence and q-dependence)

$$n^{crit} \propto \frac{P_{in}^{x}}{q_{\psi}^{1-x}} \tag{3}$$

where $x \simeq 0.5$ and $x \simeq 0$ in the power dependent and Hugill-Greenwald cases, respectively. Power dependent DL scalings have been derived from a number of different models. They are, in particular, characteristic of energy balance based models that rely in one way or other on maximum allowable radiative fractions [11], but also follow from SOL based models if the threshold condition is associated with an

approximately constant divertor temperature [4, 10]. In contrast, the only SOL based model that reproduces Hugill-Greenwald behaviour, at least under certain conditions, seems to be the one proposed in Ref. [4]. Though Ref. [4] is restricted to the physics of the high recycling regime and is thus not applicable in the presence of a gas target, it contains a rather general discussion showing that power independent, $1/q$-scalings may result from edge models if the critical condition strongly depends on the transverse (i.e. radial) collisionality of neutrals in the divertor. We consider this element to be an ingredient essential to understanding this regime and the present paper is to a large extent an attempt to generalize this idea to the situation of completely detached gas targets.

There is a relatively firm database for the power dependence and q-dependence, while information on the impact of B_t and the plasma shape is rather scarce. As already indicated by the previous discussion, we therefore adopt the position that a DL model, in order to be convincing, must at least reproduce the observed power and q-dependences.

In this context it is worthwhile mentioning the particular role of the ohmic density limit database. The loop voltage in ohmic discharges is relatively device and discharge independent so that one has for the ohmic input power $P_\Omega = U_L I_p \propto I_p \propto 1/q_\psi$. Hence, with Eq. (3), one always has $n^{crit} \propto 1/q_\psi$, irrespective of the actual power dependence. Ohmic density limit studies are therefore not particularly helpful to our discussion and will be completely ignored.

So far we have ignored the special character that the H-mode DL may have, particularly due to the existence of the H-mode threshold. We defer the detailed discussion of this aspect to Section 5.

Summarizing these introductory remarks, we thus try to understand the Hugill-Greenwald type DL scaling behaviour of divertor tokamaks within the context of a SOL based description of the fully detached state.

We start with an analytical discussion in Section 2, based on a simple two-point model which is reinforced by dimensional considerations on gas targets. In this section the underlying physics is determined and resulting scalings for different SOL transport models are derived. In Section 3 results of an extensive B2-EIRENE campaign are compared with the analytical predictions. In Section 4 we compare our modelling results with experimental findings from JET. Finally, a discussion of miscellaneous aspects is presented in Section 5.

2. ANALYTICAL DISCUSSION

2.1 Basic mechanism

Simple analytical SOL models, so-called two-point (2-P) models, have proved to be extremely useful in the attached regime. One reason for this is that neutrals have little impact on the momentum and energy balances under attached conditions. This is no longer true in the presence of a gas target [5]. In order to benefit from the analytical approach, despite the absence of analytical gas target models, we adopt an

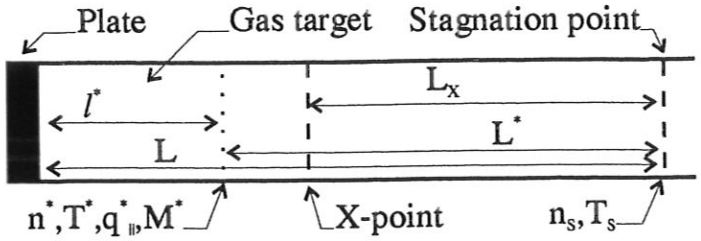

FIG. 2. *Schematic (1-D) view of the setup considered. A 2-P model is applied in the region between the stagnation point and gas target entrance (dotted vertical line). The gas target is replaced by boundary conditions at the entrance. Ionization occurs above the gas target entrance, which is also the "ionization front".*

approach first proposed in Ref. [15] by confining ourselves to the region between the ionization front and stagnation point (upstream region) and replacing the gas target by boundary conditions at the gas target entrance (see Fig. 2). In the upstream region 2-P models are well justified. Information on the gas target is obtained from dimensional considerations, which provide us with information on how particle and power fluxes at the gas target entrance depend on local density and temperature.

Versions of the basic equations of a two-point model are given in Refs [4, 10] for the case of standard sheath boundary conditions and Bohm-like perpendicular transport. We use them in the upstream region with some minor modifications to allow for arbitrary Mach number at the gas target entrance:[1]

$$n^* = \frac{1}{1+M^{*2}} \frac{n_S T_S}{T^*} \tag{4}$$

$$\Delta = \frac{5}{32} \frac{c}{e} \alpha_{D_B} \frac{n_S T_S^2}{q_\perp B_t} \tag{5}$$

$$T_S = \left(\frac{49}{4\kappa} \frac{q_\perp L^* L_X}{\Delta} \right)^{2/7} \tag{6}$$

$$\frac{7}{2} \frac{L q_\perp}{\Delta} = c_s^* n^* M^* [\xi^* + \gamma^* T^*] \tag{7}$$

Here * and $_S$ denote quantities at the gas target entrance and stagnation point, respectively. Δ is the temperature SOL thickness (in the upstream region), L^* the connection length between the stagnation point and gas target entrance, L_X the connection length between the stagnation point and X-point, and $q_\perp$ the mean power flux across the separatrix. κ determines the Spitzer parallel electron heat conductivity: $\kappa_{Spitzer} = \kappa T^{5/2}$. (The potential role of heat flux limits will be addressed in Sec. 3.) Bohm type perpendicular transport is assumed: $\chi_\perp = \alpha_{D_B} D_B$, $D_B = cT/(16eB_t)$. ξ^* is the mean energy consumed per ionization event and c_s is the ion sound speed

[1] The units are CGS units except where otherwise stated.

($c_s = \sqrt{(\mu T_i + T_e)/m}$, $\mu = 1$, $T_i = T_e$) [16]. In particular, $M^* = v_{\|}^*/c_s^*$ is the Mach number and $\gamma^* = q_{\|}/(n^* T^* c_s^*)$, where $q_{\|}^*$ is the total heat flux into the gas target, is the "generalized sheath transmission coefficient" at the gas target entrance.

Equation (4) is derived from the momentum balance equation. Equations (5) and (6) follow from local analysis of the SOL power balance, while Eq. (7) is essentially the global power balance equation in the region under consideration. The term $\frac{7}{2} L q_\perp / \Delta$ is the parallel power flux in the upstream region, which splits into the power flux into the gas target ($c_s^* n^* M^* \gamma^* T^*$) and the power consumed within the recycling process ($c_s^* n^* M^* \xi^*$). $c_s^* n^* M^*$ is the ion flux to the plate. (In this study we conveniently omit impurity radiation in the SOL, which can easily be included in parametric form [17].)

For a derivation of Eqs (4) to (7) see Ref. [4], where a more convenient form of Eq. (7) is also given:

$$n_S = \left(\frac{7}{\tilde{c}_s}\right)^{11/16} \left(\frac{32e}{5c} \frac{1}{\alpha_{D_B}}\right)^{5/16} \left(\frac{4\kappa}{49}\right)^{3/8}$$

$$\times \frac{B_t^{5/16} q_\perp^{5/8}}{L_X^{1/16}} \frac{T^{*11/32}}{[M^*(\xi^* + \gamma^* T^*)]^{11/16}} \tag{8}$$

where $c_s(T) = \tilde{c} T^{1/2}$ and the approximation $L^* \simeq L_X$ has been used.

It will be shown in Sec. 2.2 that under completely detached conditions

(i) M^* and γ^* are solely functions of the transverse neutral collisionality at the gas target entrance:

$$M^*, \gamma^* = M^*, \gamma^* \left(\frac{\Delta_n^*}{\lambda_{n-i}^*}\right) \tag{9}$$

(ii) T^* is virtually independent of any parameter ($T^* \simeq 6.5 - 7.0\ eV$) and can be considered as a constant.

Here $\lambda_{n-i}^* = \frac{1}{\sigma_{i-n} n^*}$ is the mean free path of a neutral with respect to $i - n$ collisions and σ_{i-n} is the ion-neutral cross-section (including cx and elastic collisions, $\sigma_{i-n} \approx 5 \times 10^{-15} \mathrm{cm}^2$). Δ_n is the density decay length.

Using Eqs (4) to (6), we can express Δ and n^* in terms of n_S and discharge parameters such as $q_\perp$, B_t, ...

$$\Delta = \left(\frac{5}{32}\right) \left(\frac{392}{5}\right)^{4/11} \alpha_{D_B}^{7/11} \left(\frac{1}{\kappa_0}\right)^{4/11} \left(\frac{c}{e}\right)^{7/11} \frac{L_X^{8/11} n_S^{7/11}}{q_\perp^{3/11} B_t^{7/11}} \tag{10}$$

$$n^* = \left(\frac{392}{5}\right)^{2/11} \frac{1}{T^*} \left(\frac{1}{\kappa_0} \frac{e}{c}\right)^{2/11} (q_\perp^2 L_X^2 B_t^{9/2})^{2/11} \tag{11}$$

to yield the following expression for the transverse neutral collisionality at the gas target entrance:

$$\frac{\Delta_n^*}{\lambda_{n-i}^*} = \left(\frac{5}{32}\right)\left(\frac{392}{5}\right)^{6/11} \frac{\sigma_{i-n} f f_n}{T^*} \alpha_{d_B}^{7/11}$$

$$\times \left(\frac{c}{e}\right)^{5/11} \left(\frac{\alpha_{q_\perp}}{\kappa_0}\right)^{5/11} \frac{q_\perp^{1/11} n_S^{16/11} L_X^{12/11}}{B_t^{5/11}} \tag{12}$$

Here f is the flux expansion factor at the gas target entrance and $f_n = \Delta_n^*/\Delta^*$. We assume $f_n \simeq const$ in what follows. f, f_n and α_{D_B} have been retained in Eq. (12) to illustrate the potential impact they may have, but in the following we confine ourselves to scaling relations in terms of discharge and device parameters, which are our main interest.

Combining Eq. (12) with Eqs (8) and (9), one gets

$$n_S^{det} \propto \frac{B_t^{5/16} q_\perp^{5/8}}{L^{*1/16}} T^{*11/32} \left\{ M^* \left(q_\perp^{1/11} n_S^{det\,16/11} L_X^{12/11} B_t^{-5/11} \right) \left[\xi^* + T^* \right.\right.$$

$$\left.\left. \times \gamma^* \left(q_\perp^{1/11} n_S^{det\,16/11} L_X^{12/11} B_t^{-5/11} \right) \right] \right\}^{-11/16} \tag{13}$$

Noting that ξ is only a relatively weak function of n and T [16], Eq. (13) provides a relation between the upstream density n_S^{det} at complete detachment and the device and discharge parameters B_t, $L_X \simeq \pi q_\psi R$, and $q_\perp$, respectively.[1] This is, in principle, the relation for n_S we are aiming at, but at this stage we are unable to provide an explicit expression for n_S, due to the lack of information on M^* and γ^*.

To extract further information from Eq. (13), we add as an additional element the assumption that the DL resulting from Eq. (13) is of the power law type. This is equivalent to making the ansatz

$$\frac{T^{*11/32}}{[M^*(\xi^* + \gamma^* T^*)]^{11/16}} \propto \left(q_\perp^{1/11} n_S^{16/11} L_X^{12/11} B_t^{-5/11} \right)^{-\beta 11/16} \tag{14}$$

where β is an undetermined parameter. It being known that experimentally observed DLs are well described by power law scalings, this is not a particularly critical assumption. Combining Eqs (13) and (14), we now get after some simple algebra ($L_X \propto q_\psi R$)

$$n_S \propto \frac{q_\perp^x B_t^{5/16}}{(q_\psi R)^{11/16 - x}} \quad where \quad x = \frac{10 - \beta}{16(1+\beta)} \tag{15}$$

Equation (15) defines the class of possible scalings for n_S that are compatible with completely detached conditions (and Bohm type perpendicular transport adopted

[1] From now on n_S is always taken at complete detachment and we can conveniently omit superscript ^{det}.

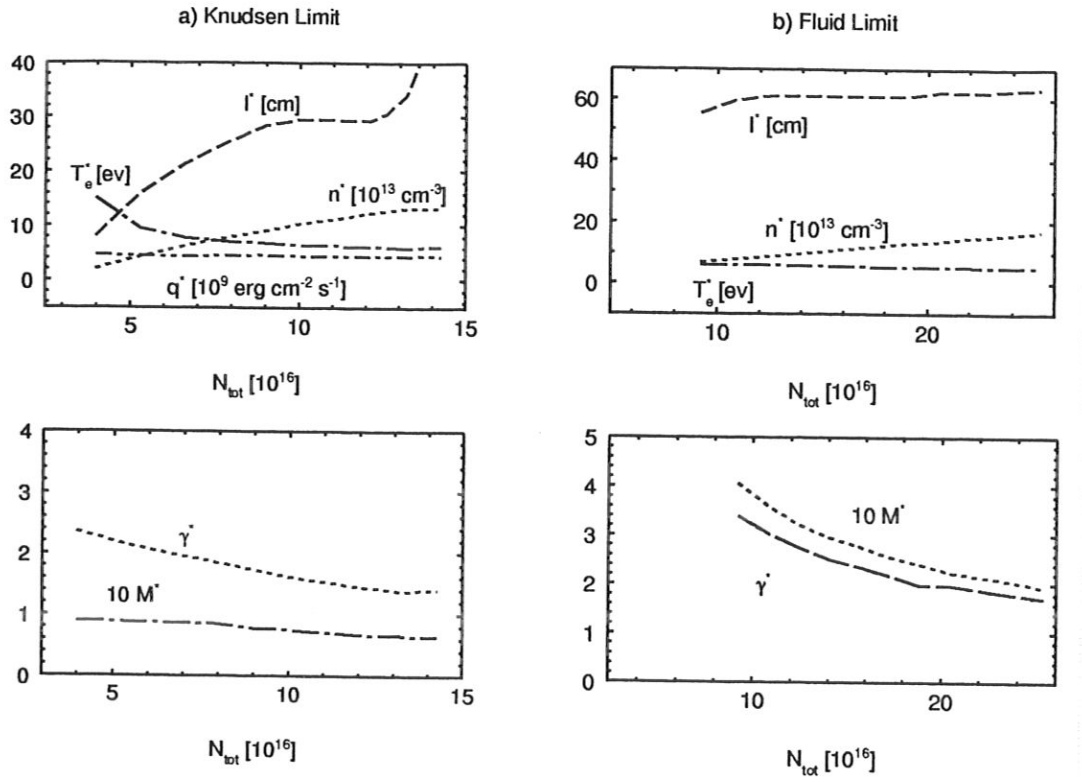

FIG. 3. *M^* and γ^* plus some other quantities of interest versus total particle content N_{tot} for a typical JET high-density discharge in the Knudsen (a) and fluid (b) regimes.*

so far). Most striking is that the correlation between the power dependence and q-dependence, as suggested by experimental findings, is essentially reproduced. Power independent and nearly $1/q$-type scalings are in particular contained in this class ($x = 0$). A somewhat arbitrary element in the discussion so far is the assumption of Bohm type perpendicular transport. It determines, in particular, the B_t-dependence, which seems to be weaker than observed. We will systematically discuss in Sec. 2.3 the impact of alternative transport models.

We can now give the condition for the existence of a power independent scaling a more physical meaning. If we take the condition $x \leq 0.2$ as a practical criterion for power independence, this requires that $\beta \geq 1.5$. Thus, a Hugill-Greenwald type DL will be observed if M^* and/or γ^* increase sufficiently strongly with increasing transverse neutral collisionality. Obviously, this can only be the case if one is in the regime of intermediate transverse collisionality.

An immediate consequence of the forms given by Eq. (9) for M^* and γ^* is that M^*, $\gamma^* \simeq const$ must hold in the very high collisionality (short mean free path, fluid) and very low collisionality (long mean free path, Knudsen) limits. However, a strong increase with Δ/λ_{n-i} in the intermediate regime requires that $M^*(\infty) >> M^*(0)$ and/or $\gamma^*(\infty) >> \gamma^*(0)$. A first indication that this is indeed the case is provided by 1-D calculations performed in the fluid and Knudsen limits. Figures 3 a) and b) show for both regimes the evolution of M^* and γ^* in a density ramp-up scenario,

modelled by an increase of the particle content. A typical detaching JET discharge is taken as study point. A more detailed discussion of the fluid regime and overall setup is given in Ref. [18], while a description of the underlying SOL-One edge code can be found in Ref. [19]. While γ^* shows little difference, M^* is considerably larger in the fluid regime, indicating an effect in the right direction.

For typical conditions at the gas target entrance one has $\xi \simeq 30-40$ so that with $T^* \simeq 6-7$ eV it is concluded from Fig. 3 that $\gamma^* T^* << \xi^*$ is marginally satisfied. Thus the dependence of M^* on transverse collisionality is the dominating factor in Eq. (13).

It is illustrative to put the previous discussion in a slightly different form. Writing

$$\frac{T^{*1/2}}{M^*(\xi^* + \gamma^* T^*)} = \frac{1}{f\left(\frac{n_S}{n_g}\right)} \tag{16}$$

where

$$n_g = c_g \frac{B_t^{5/16}}{q_\perp^{1/16}(qR)^{3/4}} \tag{17}$$

with some constant c_g (see Eq. (14)), one gets instead of Eq. (13)

$$\frac{n_S}{n_g} f\left(\frac{n_S}{n_g}\right) \propto [q_\perp q_\psi R]^{11/16} \tag{18}$$

If the function f increases sufficiently strongly in the vicinity of some value of n_S/n_g, i.e. at some transverse collisionality, as indicated schematically in Fig. 4, n_S is clamped at this ratio of n_S/n_g. Thus, the scaling in the limit of a very strong dependence of f on n_S/n_g is simply given by the condition of constant n_S/n_g, i.e. of constant transverse collisionality and

$$n_S \propto n_g \propto \frac{B_t^{5/16}}{q_\perp^{1/16}(q_\psi R)^{3/4}} \tag{19}$$

With the ansatz $f(n_S/n_g) \propto (n_S/n_g)^\beta$ we would, of course, again get Eq. (15) which transforms into Eq. (19) in the limit $\beta \to \infty$. From Eq. (18) it becomes particularly transparent why the B_t-dependence is the same for all regimes.

This section concludes with some remarks that may provide a more intuitive understanding of the strong dependence of M^* on the transverse neutral collisionality. In Ref. [6] it is shown that volume recombination plays a role under gas target conditions and that a completely detached plasma recombines in a narrow layer in front of the target. The 2-D simulations to be reported in Sec. 3 systematically show that at some point upstream from the recombination zone (as indicated by subscript c in what follows, we confine discussion to a simple 1-D picture) the parallel

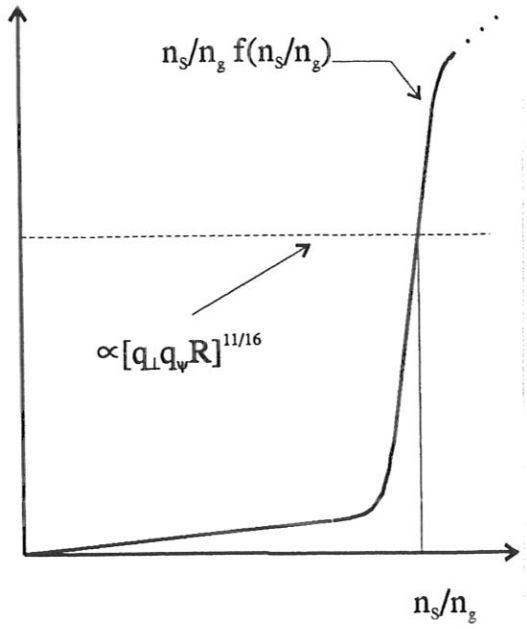

FIG. 4. *Shape of* $\frac{n_S}{n_g} f(\frac{n_S}{n_g})$ *that leads to a DL (schematic).*

heat conductivity becomes so small that the parallel heat transport becomes entirely convective. At that point one then has the relation ($T_e \simeq T_i$)

$$5T_C\Gamma_C = q_{\parallel,C} = (1-\widetilde{f})q^*_{\parallel} \tag{20}$$

where Γ_C is the ion flux at point C and $q^*_{\parallel,C}$ and $q^*_{\parallel}$ are the total heat fluxes at point C and the gas target entrance, respectively. $\widetilde{f}$ is the fraction of energy entering the gas target that is lost due to $i-n$ interactions. If C is upstream from the recombination zone there are no particle sources or sinks in the region between the gas target entrance and point C and one also has

$$\Gamma_C = \Gamma^* = v^*_{\parallel} n^* = M^* n^* c_s(T^*) \tag{21}$$

resulting in ($T^* \simeq const$)

$$M^* \propto \frac{(1-\widetilde{f})q^*_{\parallel}}{n^* T_C} \tag{22}$$

At complete detachment $(1-\widetilde{f}) << 1$ must hold (energy detachment). Furthermore, the transition to convective transport occurs in a relatively narrow temperature band at about 2eV. Finally, the transverse collisionality mainly depends on density (see Eq. (12)). Therefore, if n^* is increased by a small amount $\widetilde{f}$ will decrease by a small amount since the $i-n$ induced energy transport decreases. The denominator of the above equation will only moderately change. However, if $(1-\widetilde{f}) << 1$, the small decrease of $\widetilde{f}$ will strongly enhance $1-\widetilde{f}$ and consequently M^*.

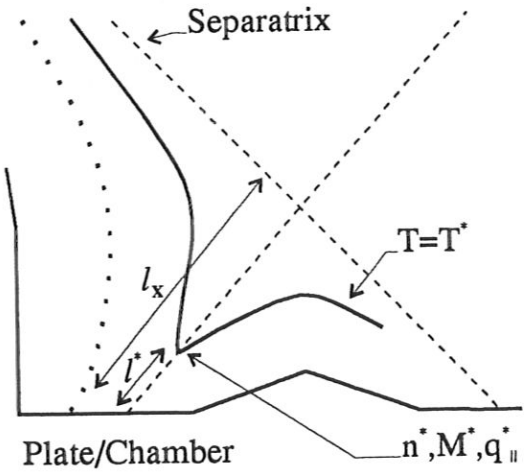

FIG. 5. *Schematic view of the setup considered for the dimensional considerations.*

It remains to be shown that present-day tokamaks are actually in the regime of intermediate collisionality, and this question will be addressed in Secs 3 and 4. An interesting consequence of the preceding discussion is that this should automatically be the case if energy detachment is achieved.

2.2 Dimensional considerations on gas targets

In this subsection we derive Eq. (9) from dimensional considerations. We apply these to the region (see Fig. 5) between the $T = T^*$ contour, which defines the gas target entrance and the plate (for the definition of T^* see below). In Fig. 5, ℓ_X is the X-point to plate distance along B, while ℓ^* is the distance along B between the tip of the $T = T^*$ contour and the plate. The following simplifying assumptions are made:

(i) The ionization rate S_i is approximated by a step function $S_i = \theta(T - T^*)S_i^0$, where T^* and S_i^0 are constants. This implies that the ionization source peaks at $T = T^*$ and that all ionization events occur upstream from the $T = T^*$ contour (ionization front).

(ii) $T_e^* \simeq T_i^* \equiv T^*$ (i.e. the electron and ion temperatures are nearly equal at the ionization front).

(iii) Transport in the gas target is dominated by $i - n$ and Coulomb collisions.

(iv) Momentum and energy transfer by neutrals to the wall is perfect (i.e. a neutral leaving the plasma loses all its momentum and energy at the wall).

(v) Other than two-body processes (three-body volume recombination, multistep ionization processes) are ignored.

Because of the steep increase of S_i with T_e in the 5eV range, assumption (i) is a good approximation. In fact, numerical simulations always show that nn_0S_i peaks at about 6.5eV and sharply drops toward lower temperatures. Assumption (ii) is

well satisfied under normal tokamak conditions due to the relatively high densities at the gas target entrance. Assumption (iii) excludes widening of the SOL width due to anomalous perpendicular transport. Finally, by making assumption (iv) we remove neutral-neutral collisions as well as the chamber width from the problem. Assumption (v) will be discussed below in greater detail.

With these simplifications a solution of the standard fluid SOL equations which is valid in the gas target region (i.e. between the plate and ionization front) is determined by, for instance, the following quantities (from now on we follow Ref. [20]):

- T^* temperature at the ionization front
- n^* separatrix density at the ionization front
- m ion mass
- e elementary charge
- σ_{i-n} ion neutral cross-section (cx and elastic)
- Δ_n^* SOL width (e.g. density SOL width)
- ℓ^* distance (along B) from the tip of the $T = T^*$ contour to the plate
- ℓ_X plate to X-point distance along B
- ψ^0 field line pitch (e.g. some mean value)

We suppress in this list dimensionless quantities such as m_e/m_i or γ_i and γ_e (sheath transmission coefficients) which are determined by elementary constants or are approximately constant, as well as profile factors characterizing the shape of n at the gas target entrance, which are assumed to be fixed.

From these 9 parameters we can form the following 9-3=6 dimensionless combinations:

$$
\begin{aligned}
n^* \sigma_{i-n}^{*3/2} &\longleftrightarrow \frac{\sigma_{i-n}^{*1/2}}{\lambda_{n-i}^*} \\
\frac{T^{*2} \sigma_{i-n}}{e^4} &\longleftrightarrow \frac{\lambda_{Coulomb}}{\lambda_{n-i}^*} \\
n^* \sigma_{i-n} \ell^* &\longleftrightarrow \frac{\ell^*}{\lambda_{n-i}^*} \\
n^* \sigma_{i-n} \ell_X &\longleftrightarrow \frac{\ell_X}{\lambda_{n-i}^*} \\
n^* \sigma_{i-n} \Delta_n^* &\longleftrightarrow \frac{\Delta_n^*}{\lambda_{n-i}^*} \\
\psi^0 &\longleftrightarrow \psi^0
\end{aligned}
$$

where λ_{n-i}^* and $\lambda_{Coulomb}^*$ are, respectively, the mean free paths with respect to ion-neutral and Coulomb collisions. Any other dimensionless combination, such as $q_\parallel^* m^{1/2} n^{*-1} T^{*-3/2}$, which is basically γ^*, is then determined by the above set of parameters [20]:

$$
\gamma^* = \gamma^* \left(\frac{\Delta_n^*}{\lambda_{n-i}^*}, \frac{\ell^*}{\lambda_{n-i}^*}, \frac{\ell_X}{\lambda_{n-i}^*}, \frac{\sigma^{1/2}}{\lambda_{n-i}^*}, \frac{\lambda_{Coulomb}^*}{\lambda_{n-i}^*}, \psi^0 \right) \tag{23}
$$

A couple of arguments can be applied to put Eq. (23) in a more explicit form: As has been shown in Ref. [21], the dependence on $\sigma_{i-n}^{*1/2}/\lambda_{n-i}^*$ must disappear in the case of binary collisions. Also, $\lambda_{Coulomb}^*/\lambda_{n-i}^*$ is a function of T^* only, which can be considered as constant, so that $\lambda_{Coulomb}^*/\lambda_{n-i}^*$ can be ignored in Eq. (23). Furthermore, under low-temperature, high-density conditions one always has $\ell_X/\lambda_{n-i}^* >> \sin\psi^0 \ell_X/\lambda_{n-i}^* >> 1$. (Actually, the second part of the inequality implies that neutrals cannot reach the separatrix travelling through the divertor plasma, which is a design requirement that has to be fulfilled by any reasonable divertor.) Hence, in practice the dependence of the third argument in Eq. (23) can be neglected as well. Finally, we can remove one more variable if we consider Eq. (23) at some threshold, such as complete detachment. Removing ψ^0, we get at the threshold the form

$$\gamma^* = \gamma^* \left(\frac{\Delta_n^*}{\lambda_{n-i}^*}, \frac{\ell^*}{\ell_X} \right) \tag{24}$$

When complete detachment is achieved, the plasma no longer experiences the target and γ^* must become independent of the target position. Hence, at complete detachment the ℓ^*/ℓ_X dependence must also vanish in Eq. (24) and we get the following final form:

$$\gamma^* = \gamma^* \left(\frac{\Delta_n^*}{\lambda_{n-i}^*} \right) \tag{25}$$

which was used in the previous section.

Obviously, the same chain of arguments applies to M^* as well.

The reasoning that led to Eq. (25) is no longer valid if (three-body) recombination or multistep ionization plays a role [22]. However, as has been demonstrated in Ref. [6] for a particular case, recombination basically affects the particle balance near the plate, while the solutions are otherwise unaffected. This is true particularly in the vicinity of the ionization front, which is what we are mainly interested in. We take this as an indication that, though volume recombination is important in principle, it does not affect the way the gas target is "seen" by the upstream SOL and may therefore be ignored in the present discussion. According to our setup all ionization processes occur upstream from the gas target entrance so that multistep ionization does not affect our consideration.

2.3 Impact of perpendicular transport

To generalize the perpendicular transport model used so far, we adopt the general format for the heat diffusivity $\chi_\perp$ that has evolved in the scale-invariant approach to confinement scaling [23]:

$$\chi_\perp = D_B F(\rho^*, ...) \tag{26}$$

Here D_B is the Bohm diffusivity and ρ^* the normalized Larmor radius. F is a function which depends on, apart from ρ^*, other dimensionless quantities which describe

the effects that determine the transport. The generalized transport according to Eq. (26) is easily implemented in the basic equations given in Sec. 2.1 for Bohm-like perpendicular transport by making the substitution $B_t \rightarrow B_t F^{-1}$.

For convenience we make the popular ansatz [23]

$$F = F_0 \rho *^{\mu} \tag{27}$$

where different values of μ indicate different characteristic length scales λ of the underlying turbulent transport. In particular, $\mu = 1, 0, -1$ correspond to gyro-Bohm scaling ($\lambda \approx \rho$), Bohm scaling ($\lambda \approx a$) and stochastic diffusion ($\lambda >> a$), respectively. We assume $F_0 = const$, thus ignoring possible residual dependences on other parameters. With

$$\rho^* \propto \frac{T_S^{1/2}}{RB_t}$$

and by expressing T_S in terms of n_S and discharge parameters such as n_S, $q_\perp$, etc. by means of Eqs (5) and (6), we obtain a generalized version of Eq. (12) for the transverse collisionality in the presence of generalized perpendicular transport according to Eq. (27)

$$\frac{\Delta}{\lambda^*_{n-i}} \propto \left[\frac{n_S^{(16+\mu)} q_\perp^{(1+\mu)} L^{*(12-3\mu)}}{B_t^{5(1+\mu)}} \right]^{1/(16+\mu)} \tag{28}$$

and, in accordance with the logic of Eqs (16) to (19),

$$n_S \propto \left[\frac{B_t^{5(1+\mu)}}{q_\perp^{(1+\mu)} L^{*(12-3\mu)}} \right]^{1/(16+\mu)} \tag{29}$$

in the regime of intermediate transverse collisionality.

An important consequence of Eq. (29) is that the B_t and L_X-dependences are adversely affected. For gyro-Bohm scaling one has, for instance, $n_S \propto B_t^{10/17}$ but only $n_S \propto L_X^{-9/17}$, which is clearly in contradiction with what is observed experimentally.

A model not covered by Eqs (26) and (27) uses $\chi_\perp = const$. Though lacking any theoretical basis, it is widely used in numerical SOL studies. When comparing in Sec. 3 the analytical predictions with numerical results, we also partly rely on this model. In that context it is mainly relations similar to Eq. (15), which describe the general class of scalings compatible with a transport model, that are of interest. By complete analogy with the Bohm case one gets for $\chi_\perp = const$ instead of Eq. (15)

$$n_S \propto \frac{q_\perp^x}{(q_\psi R)^{9/14-x}} \quad where \quad x = \frac{10+\beta}{14(1+\beta)} \tag{30}$$

where the relation

$$\frac{T^{*11/32}}{[M^*(\xi^* + M^{*2}\gamma^* T^*)]^{11/16}} \propto \left(q_\perp^{-1/9} n_S^{14/9} L_X^{8/9} \right)^{-\beta 9/14}$$

replaces Eq. (14). Of course, Eq. (30) does not contain any B_t-dependence. For the same power dependence (x value), the q-dependence is somewhat weaker than in the Bohm case. Also the dependence of x on β is weaker than in the Bohm case. Now $\beta \geq 4$ is required to get $x \leq 0.2$.

3. B2-EIRENE SIMULATIONS

In the preceding section we derived scaling relations for the upstream separatrix density on the assumption of an intermediate transverse collisionality in the divertor when complete detachment is reached. 2-D codes offer, at least for particular cases, the possibility to assess the validity of this assumption and check the scalings derived from the simple models. In this section we summarize the results of an extensive B2-EIRENE [24, 25] campaign that was conducted along these lines.

JET discharge 30829 is adopted as study point [26]. The original magnetic configuration and, except for gaps, the MARK-I divertor and first wall shapes are used in the simulation. In order to avoid the complication of varying impurity radiative fractions, we confine ourselves to a pure deuterium case. The incoming power is evenly distributed between electrons and ions. $q_{95\%} = 3.6$ for this configuration.

In the simulations we approach complete detachment by performing a sequence of B2-EIRENE runs to steady state, successively increasing the particle content N_{tot} (ions + neutrals) at otherwise fixed input parameters. Complete detachment is defined as the point at which in the inner divertor about 80% of the ionized neutrals recombine by volume recombination, which is typically associated with a drastic drop of both the power and particle fluxes to the plate. For the same configuration the detached state and the transition to it have been described in greater detail in Ref. [6] with particular emphasis on the role of volume recombination in detachment. We can therefore confine ourselves to a discussion of those aspects that directly relate to the topic of this paper.

Modelling of detached, recombining divertors is rather demanding as regards computer resources. For the purely economical reason of using runs performed previously in a different context, we present (except where otherwise stated) results that were obtained with constant transverse particle and heat diffusivities ($D_\perp = 0.2\ m^2/s$, $\chi_\perp = 1.0\ m^2/s$).

In all runs heat flux limits were turned off. A representative selection of cases were performed with and without flux limits but no difference was observed. This agrees with the expectation that the importance of kinetic flux limits should decrease for higher densities.

We begin with Fig. 6, which illustrates how n_S evolves during a density ramp-up for three different input powers. Figure 6, in particular, shows that n_S, taken at complete detachment, depends only weakly on P_{in}.

The result of a complete power scan and q-scan (1.8 MW $\leq P_{in} \leq$ 3.6 MW, $2.4 \leq q_{95} \leq 5.4$) is summarized in Fig. 7. The scaling is well described by the relation $n_S \propto P_{in}^{0.15}/q_{95}^{0.7}$, which is consistent with Eq. (30) except that, for the observed power dependence, the q-dependence is somewhat stronger than predicted by the analytical

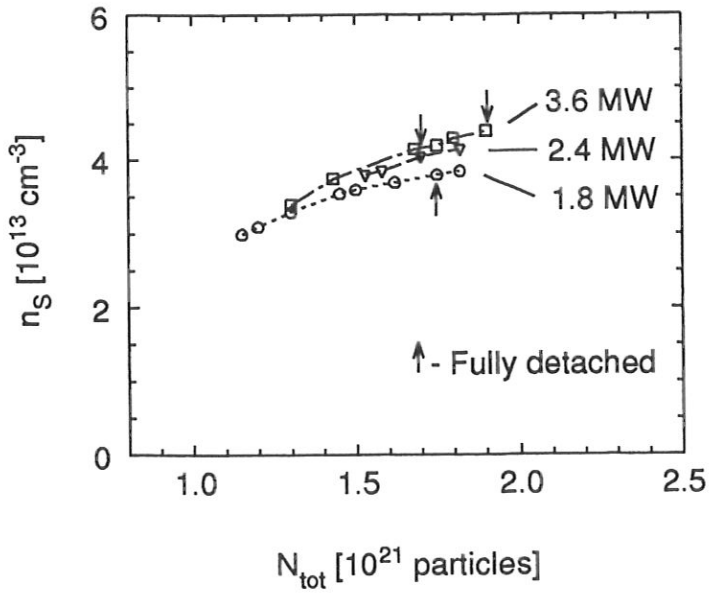

FIG. 6. *Upstream density n_S versus total particle content N_{tot} for three different input powers and constant perpendicular transport.*

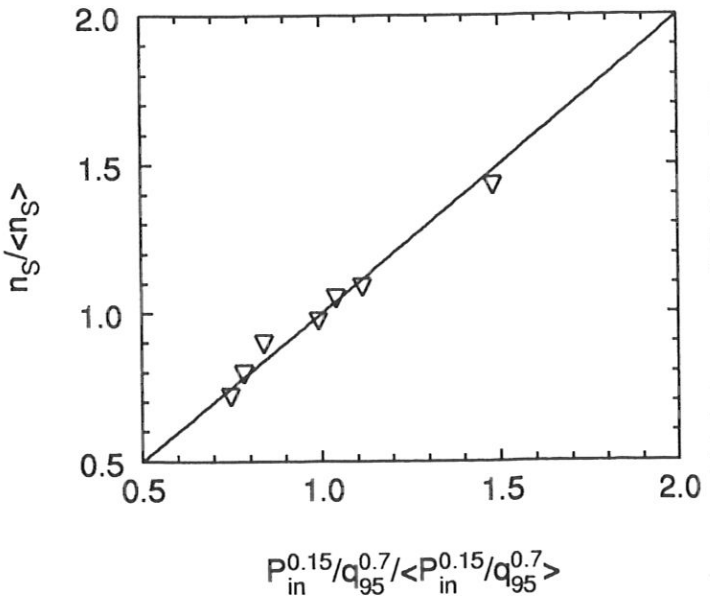

FIG. 7. *Summary of numerical scaling study (power scan and q-scan for constant perpendicular transport). < .. > denotes an ensemble average.*

considerations. This is a general phenomenon and is most likely a consequence of the approximation $\xi \simeq const$ made in Sec. 2.1. In the light of the results of Sec. 2.3, one would expect a somewhat weaker $q_\perp$ dependence and a somwhat stronger q_ψ dependence if Bohm type perpendicular transport is applied.

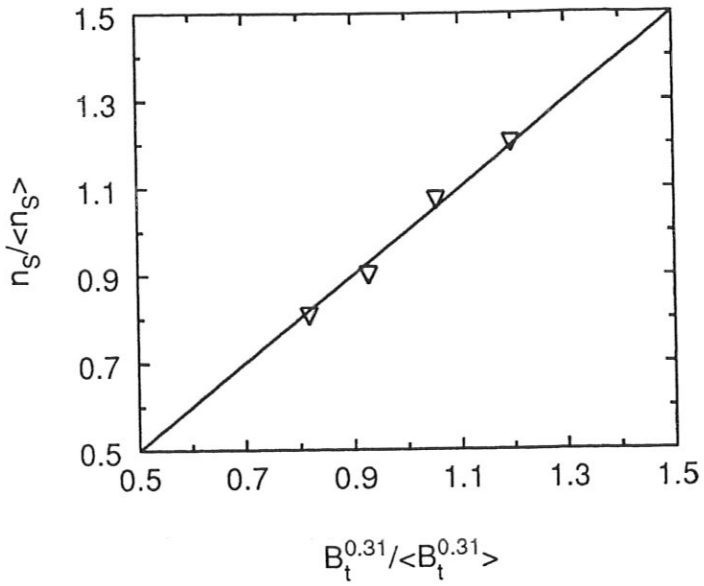

FIG. 8. *Summary of numerical B_t-scaling study for Bohm type perpendicular transport. B_t = 1.6, 2.4, 3.6 and 5.4T. < .. > denotes an ensemble average.*

In order to check the B_t-dependence, we performed a separate B_t-scan using $\chi_\perp = D_{Bohm}(\equiv \frac{cT_e}{16eB_t})$ and $D_\perp = 0.2\chi_\perp$ for an intermediate power P_{in} = 2.4MW and q_ψ = 3.6 (reference case). The result is plotted in Fig. 8, which shows that the analytically predicted B_t-dependence is reproduced as well. It is worthwhile mentioning that both transport options lead to remarkably similar solutions.

These results suggest that the criterion for a weak power dependence as formulated in Sec. 2.1 is fulfilled and the scaling relations derived from the simple model are well reproduced by the 2-D simulations.

4. COMPARISON WITH EXPERIMENT

We present a comparison with some completely detached JET discharges obtained with the MARK-I divertor configuration, which was already used for the 2-D modelling in Sec. 3. While most of the discharges are terminated by a disruption, some stay, as a result of careful discharge tailoring, in the detached state until regular termination. In these cases the density shows a plateau. The database includes L-mode and a small number of H-mode discharges. Detached H-modes in JET require careful impurity injection [27]. P_{heat} (heating power), B_t and q_ψ vary, respectively, in the ranges 3.4MW$\leq P_{heat} \leq$18.2MW, 2.05T$\leq B_t \leq$2.82T and 2.98$\leq q_\psi \leq$4.93. JET does not provide separatrix upstream densities under high-density conditions and we have to use the line averaged density instead, assuming a constant peaking factor. In Figs 9a and b line averaged densities measured at complete detachment (n^{exp}) are plotted versus a weakly power dependent Hugill-Greenwald scaling ($n \propto q_{\perp,eff}^{0.1} B_t/q_\psi$) and the scaling derived in Secs 2 and 3 for Bohm type perpendicular transport

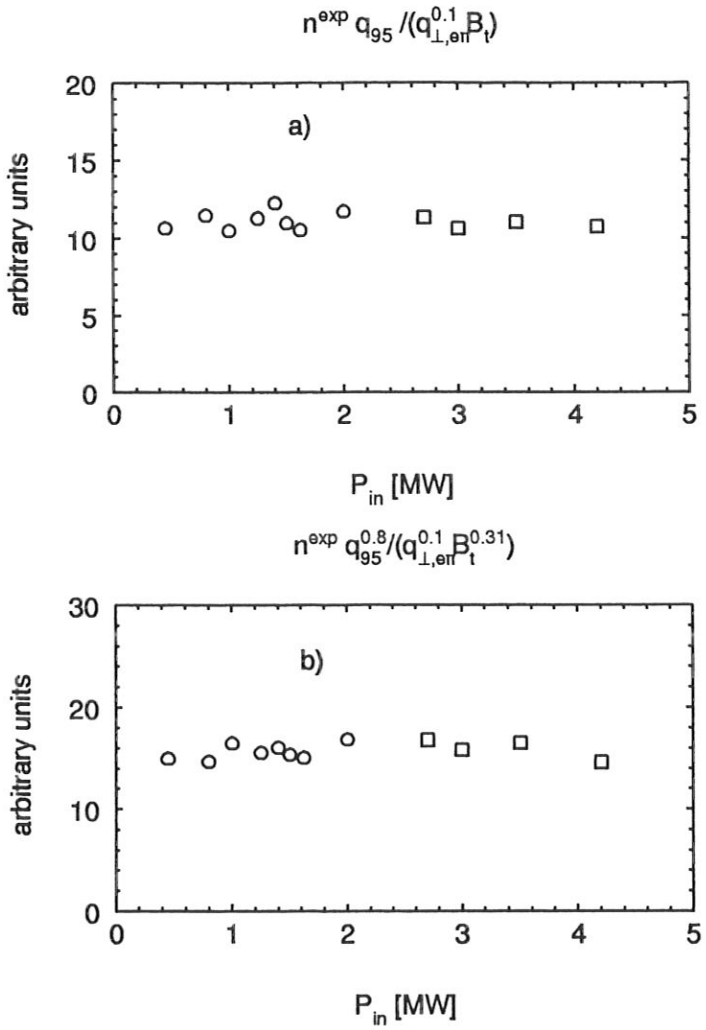

FIG. 9. *Comparison of various density limit scalings with completely detached JET discharges. Plotted (in arbitrary units) is the ratio of the measured line averaged density at complete detachment n^{exp} and the predicted density versus net input input power $P_{in} = P_{heat} - P_{rad}^{tot}$, which is used as a label: (a) Weakly power dependent Hugill-Greenwald scaling. (b) Proposed scaling for Bohm type transverse transport. The database includes L-mode (diamonds) and H-mode (squares) discharges.*

($n \propto q_{\perp,eff}^{0.10} B_t^{0.31}/q_\psi^{0.8}$), where $q_{\perp,eff} = (P_{heat} - P_{rad}^{tot})/O_p$, following a discussion in Ref. [27]. There it was shown for the attached regime and using a version of the 2-P model that accounts for divertor impurity radiation that n_S is virtually independent of how P_{rad}^{tot} splits into core and SOL radiation. Adaptation of this argument to the detached regime is straightforward.

There is no visible difference in the quality of the fit for the two cases, but the range of B_t and q_ψ variation is somewhat limited. The quantitative values obtained in Sec. 3 for n_S are typically 20-30% lower than the line averaged densities measured

under similar conditions. In view of the fact that LIDAR measurements show flat density profiles in the interior of the core, this is at least not inconsistent.

Recent lithium beam measurements of the maximum upstream separatrix density in ASDEX Upgrade show an approximately square root power dependence, indicating that ASDEX Upgrade operates in a different regime. We will come back to this point in Sec. 5.

5. SUMMARY AND DISCUSSION

We have investigated the upstream separatrix density in a tokamak at complete detachment. Experimental evidence has been discussed that this is typically the maximum achievable edge density and thus defines the density limit. Scaling relations for this limit were derived from simple two-point models and dimensional considerations. The main interest of the paper was in power independent, $1/q$-type scalings that are observed in most divertor tokamaks. We have shown that this type of scaling results if the divertor is in the regime of intermediate transverse collisionality for neutrals. Extensive B2-EIRENE simulations for a typical JET configuration were performed to assess that this condition is actually achieved and the analytically predicted scaling is reproduced. In what follows we briefly discuss some of the assumptions made, the relation to other DL models and empirical scalings, possible ways to overcome the limit, and future work.

A certain weakness of SOL based DLs stems from the fact that a B_t-dependence (at constant q_ψ and $q_\perp$) can only enter through a B_t-dependence of $\chi_\perp$ and $D_\perp$. As discussed in Sec. 2.2, among the transport models currently considered only Bohm-like transport results in DL scalings which are in acceptable agreement with the well established parts of the database. The assumptions on $\chi_\perp$ and $D_\perp$ can be validated directly by comparing them with SOL measurements or indirectly by checking the scalings derived.

As regards direct measurements one has to be aware of the fact that (see Sec. 2) it is the power scrape-off layer that counts in this context. Thus only transport in the first $3-5$mm of the SOL is important. Taking, for instance, the usual uncertainties about the separatrix position, it is certainly difficult to measure n, T and decay lengths directly to determine $\chi_\perp$ and $D_\perp$ with sufficient accuracy. Also, since convective perpendicular energy transport is usually negligible, all density fall-off length measurements, which earn particular attention, are irrelevant in this context.

Indirect determination would require DL scans with varying B_t field. Unfortunately, the database is very poor in this respect. Only very few explicit checks of the B_t-dependence have been discussed in the literature. In JET beryllium limiter discharges the B_t-dependence seems to be relatively weak and consistent with our prediction [10]. Also some ASDEX observations point in this direction [28]. There are more data for ohmic discharges [9], but, as expounded in Sec. 1, they are inconclusive. We therefore adopt the position that the present database is not in contradiction to the scaling proposed here and that further R&D is needed to resolve this issue.

Concerning the dependence on the plasma shape, which constitutes the main dif-

ference between the Hugill and Greenwald scalings, the situation is similar. A number of dedicated studies have been performed to discriminate between the two options which are not fully conclusive. We, therefore, again consider this an open question that awaits improvement of the database. It is, however, worthwhile mentioning that most current (elongated) tokamaks report density limits somewhat below Greenwald. This would be an immediate consequence if the Hugill type elongation dependence were the more appropriate one. Consistently with this suspicion, the data given in Ref. [29] for the nearly circular ASDEX tokamak agree exactly with the Greenwald scaling.

The key element of the present paper is the assumed coincidence of complete detachment with the achievement of the maximum edge density. Though 2-D modelling provides a lot of evidence for this, we have relied on experimental evidence. A full exploration of these aspects would have to include the dynamics of Marfes and the potential role of MHD effects in the outer core plasma and would exceed the scope of this paper.

At the present stage we cannot definitely exclude that, at least in certain parameter ranges, competing mechanisms become effective prior to complete detachment. Experimentally one quite often finds, for instance, deviations from the normal scaling behaviour for very high and very low q-values.

A striking example of a competing mechanism is the H-mode threshold. Though it is not normally perceived in this way, it could be interpreted as a non-disruptive DL. In a wide parameter range the H-mode threshold is attained before complete detachment is reached. However, completely detached H-modes have been achieved in discharges with carefully controlled impurity injection [30]. The accessibility of the detached H-mode, which depends on a number of factors, has been systematically discussed in Ref. [27]. In the complete detachment regime all our considerations apply, except possibly for a difference in transport. However, at complete detachment the H-mode state seems to become indistinguishable from the L-mode state as far as global parameters are concerned [30], indicating that even the transport properties become similar. In this sense we do not expect any difference between the L and H-mode, except that in the H-mode the H to L boundary appears as a competing mechanism, but a more detailed inspection of the database is needed to confirm this. We emphasize that the results presented in Sec. 4, which include L-mode and completely detached H-modes, support this view.

The question of how to overcome the proposed DL has two distinct aspects, namely whether there are model immanent conditions that allow higher densities and whether other limiting mechanisms take over once a route to higher densities has been identified. We start with a discussion of the first aspect. It is clear that, whenever a divertor is in the regime of intermediate collisionality, the described mechanism is very robust and higher upstream densities could only be obtained in the high and low collisionality regimes, where a positive power dependence offers the possibility to increase n_S by increasing the input power (see Eq. (13)). It is obvious that, unlike the limiter case, the low collisionality conditions are inaccessible under detached divertor conditions and one is left with the question whether high collisionality conditions can be achieved. Generally $\Delta_n^*/\lambda_{n-i}^* \propto n^*\Delta_n^*$. Δ_n^* can increase because of high perpendicular transport or by a divertor configuration with high flux expansion

($f >> 1$, see Eq. (12)). Because of the second effect short divertors (low X-point to plate distance) could be potential candidates for this regime. Also, controlling recycling by a specific divertor design may lead to a widening of the density profile (increase of f_n in Eq. (12)). n^* increases with increasing power into the gas target ($q_{\|}^*$, see eq. (11) and note that $q_{\|}^* \propto q_{\perp}$ in our model). However, in reality $q_{\|}^*$ is not freely controllable, since natural impurity radiation increases with increasing n^* and n_S and completely detached H-modes require impurity injection [27]. In JET, for instance, even for highest heating powers, the power into the gas target barely exceeds $4 - 5$MW. An interesting example for a power dependent regime is provided by the ASDEX Upgrade measurements already mentioned in Sec. 4. Of the discussed causes all may play a role, particularly the comparatively high energy flux densities into the gas target achieved in ASDEX Upgrade. The detailed assessment is underway and will be presented elsewhere [31]. Accessibility of the power dependent regime is of particular importance for ITER which has to operate at core densities well above the classical Greenwald limit [32]. If one succeeds in bypassing the regime of intermediate collisionality, other mechanisms may become effective and what was said above on competing mechanisms applies here.

In principle, there may also be limits on the line averaged density. A trivial example is provided by the condition of 100% bulk radiation, which at least in limiter machines [11] or limiter-like X-point discharges may play a role. On the other hand, recent pellet studies on ASDEX Upgrade [33] have shown that the line averaged density can be significantly increased over its value in gas puffed discharges without affecting the maximum edge density, indicating that there is no bulk plasma based limiting mechanism just behind the currently observed edge limits.

Future studies will concentrate on improving understanding of the range of applicability of the proposed model with a view to obtaining access to a power dependent regime. A detailed investigation of ASDEX Upgrade, where this regime seems to exist, is particularly promising in this respect.

ACKNOWLEDGEMENT

The authors gratefully acknowledge discussions with K. Lackner, M. Kaufmann, J. Neuhauser, D. Coster, V. Mertens, G. Vlases and A. Loarte. Support by V. Mertens in evaluating ASDEX Upgrade data is particularly acknowledged. A. Loarte and R. Monk were very helpful in compiling the JET discharges.

REFERENCES

[1] WESSON, J.A., GILL, R.D., HUGON, M., et al., Nucl. Fusion **29** (1989) 641.

[2] STÄBLER, A., NIEDERMEYER, H., LOCH, R., et al., in Controlled Fusion and Plasma Physics (Proc. 16th Eur. Conf. Venice, 1989), Vol. 13B, Part I, European Physical Society (1989) 23.

[3] LOWRY, C.G., CAMPBELL, D.J., GOTTARDI, N., LAWSON, K., VLASES, G., in Controlled Fusion and Plasma Heating (Proc. 17th Eur. Conf. Amsterdam, 1990), Vol. 14B, Part I, European Physical Society (1990) 339.

[4] BORRASS, K., Nucl. Fusion **31** (1991) 1035.

[5] STANGEBY, P.C., Nucl. Fusion **33** (1993) 1695.
[6] BORRASS, K., COSTER, D., REITER, D., SCHNEIDER, R., Study of Recombining Gas Targets, to be published in J. Nucl. Mater (Proc. 12th Int. Conf. on Plasma Surface Interactions in Controlled Fus. Devices, PSI, St. Raphael, 1996).
[7] AXON. K.B., et al., in Plasma Physics and Controlled Nuclear Fusion Research 1980 (Proc. 8th Int. Conf. Brussels, 1980), Vol. 1, IAEA, Vienna (1981) 413.
[8] GREENWALD, M., TERRY, J.L., WOLFE, S.M., et al., Nucl. Fusion **28** (1988) 2199.
[9] PETRIE, T.W., et al., Nucl. Fusion **33** (1993) 929.
[10] BORRASS, et al., Nucl. Fusion **33** (1993) 63.
[11] SCHÜLLER, F.C., Plasma Phys. Control. Fusion **37** (1995) A135-A162.
[12] BELL, M.G., et al., Nucl. Fusion **32** (1992) 1585.
[13] WAIDMANN, G., KUANG, G., Nucl. Fusion **32** (1992) 645.
[14] NIEDERMEYER, H., et al., in Controlled Fusion and Plasma Physics (Proc. 12th Europ. Conf. Budapest, 1985), Vol. 9F, Part I, European Physical Society (1985) 159.
[15] BORRASS, K., STANGEBY, P.C., in Controlled Fusion and Plasma Physics (Proc. 20th Eur. Conf. Lisbon, 1993), Vol. 17C, Part II, European Physical Society, Geneva (1993) 763.
[16] HARRISON, M.F.A., in Physics of Plasma-Wall Interactions in Controlled Fusion (POST, D. E., BEHRISCH, R., Eds), Plenum Press, New York and London (1986).
[17] BORRASS, K., JANESCHITZ, G., Nucl. Fusion **34** (1994) 1203.
[18] BORRASS, K., HUYSMANS, G.T.A., in Controlled Fusion and Plasma Physics (Proc. 22th Eur. Conf. Bournemouth, 1995), Vol. 19C, Part I, European Physical Society, Geneva (1995) 341.
[19] HUYSMANS, G.T.A, BORRASS, K., SOL-One, A 1-D Scrape-off Layer Transport Code, Report JET-R(96)06, JET Joint Undertaking, Abingdon.
[20] SEDOV, L.I., Similarity and Dimensional Methods in Mechanics, Academic Press Inc., New York (1959).
[21] LACKNER, K., Comments Plasma Phys. Controlled Fusion **15** (1994) 359.
[22] CATTO, P.J., et al., Report PFC/JA-96-6, MIT Plasma Fusion Center, Cambridge, Massachusetts (1996).
[23] CHRISTIANSEN, J.P, et al., Nucl. Fusion **31** (1991) 2117.
[24] SCHNEIDER, R., et al., J. Nucl. Mater. **196-198** (1992) 810.
[25] REITER, D., J. Nucl. Mater. **196-198** (1992) 80.
[26] HORTON, L.D., and JET Team, in Plasma Physics and Controlled Nuclear Fusion Research 1994 (Proc. 15th Int. Conf., Seville, 1994), paper IAEA-CN-60/A4-I-5.
[27] BORRASS, K., FARENGO, R., VLASES, G., Report JET-P(95)74, JET Joint Undertaking, Abingdon, Oxfordshire (1994), accepted for publication in Nuclear Fusion.
[28] NIEDERMEYER, H., et al., in Controlled Fusion and Plasma Physics (Proc. 12th Europ. Conf. Budapest, 1985), Vol. 9F, Part I, European Physical Society (1985) 159.
[29] STÄBLER, A., et al., in Controlled Fusion and Plasma Heating (Proc. 17th Eur. Conf. Amsterdam, 1990), Vol. 14B, Part I, European Physical Society (1990) 395.
[30] NEUHAUSER, J., et al., Plasma Phys. Control. Fusion **37** (1995) A37-A51.
[31] MERTENS, V., et al., 16th IAEA Fusion Energy Conf. Montreal, 1996, paper IAEA/CN/64/A2-4
[32] JANESCHITZ, G., et al., Plasma Phys. Control. Fusion **37** (1995) A19-A35.
[33] MERTENS, V., et al., High Density Operation in Auxiliary Heated ASDEX Upgrade Discharges, to be published in Controlled Fusion and Plasma Physics (Proc. 23th Eur. Conf. Kiev, 1996).